Heliyon 10 (2024) e39956

Contents lists available at ScienceDirect

Heliyon

journal homepage: www.cell.com/heliyon

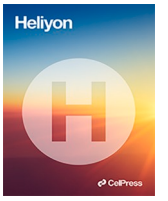

Research article

Load recognition of connecting-shaft rotor system under complex working conditions

Kun Zhang *, Zhaojian Yang

College of Mechanical Engineering, Taiyuan University of Technology, Taiyuan, 030024, China

ARTICLE INFO

Keywords:
Feature extraction
Load recognition
Rotor system
Information fusion

ABSTRACT

A method for qualitatively recognizing the load of the rolling equipment's connecting-shaft rotor system is proposed in this paper due to the complexity of rolling production conditions and the limitations of single source response signals. The method is oriented towards fusing the vibration and motor's current information. First, singular value decomposition and wavelet packet analysis are used to preprocess the two types of response signals. Then, the Bayesian estimation method in feature-level fusion achieves qualitative recognition and analysis of rotor system load types. Corresponding load experiments are completed on a load recognition test platform based on vibration and the motor's current signals. The research results show that the load recognition method based on fusion information can recognize the type of load excitation with a recognition accuracy of 91.7 %, higher than other single-source response signal methods. Therefore, the feasibility of the aforementioned theoretical methods is verified.

1. Introduction

The rolling industry is an important basic industry of the national economy, an important indicator of economic level and comprehensive national strength. The loading conditions of the rolling equipment's connecting-shaft rotor system are relatively complex, such as withstanding steady loads during constant speed operation, impact loads during starting and stopping, linear loads on slopes when the plate is thick, and harmonic loads when the rolled piece slips. These conditions affect the stability equipment structure, work safety, and the quality of rolled parts [1]. Therefore, various load situations that the system is subjected to must be understood and recognized, denoted as "load recognition". Load recognition refers to the deduction of system excitation based on the known system response and characteristics. Load recognition is the second type of inverse problem in dynamics [2]. There are usually two methods for determining loads in practical situations: direct measurement and load recognition [3]. Since obtaining direct monitoring methods for current loads is unsuitable due to the limitations of on-site conditions, loads must be recognized by testing the dynamic response of the system under dynamic loads [4,5]. Therefore, determining the load situation of the operating system is a difficult point in practical engineering [6], prompting researchers to conduct investigations. Movahedian et al. [7] investigated the problem of determining lateral loads on Kirchhoff plates. Hwang et al. [8] assessed modal loads and parameters in reverse for modal response systems based on their response signals. Bartlett et al. [9] proposed using the response measurement method to recognize the forces on the helicopter hub. Petersen et al. [10] measured the vibration data of a suspension bridge and employed the reaction force method to determine the wind loads on the bridge. This method was proven to be more deterministic than the traditional research

* Corresponding author.
E-mail address: zhangkun@tyut.edu.cn (K. Zhang).

https://doi.org/10.1016/j.heliyon.2024.e39956
Received 26 October 2024; Accepted 28 October 2024
Available online 30 October 2024

methods. Therefore, this paper is based on experimental measurement information to recognize the load excitation of the rotor system.

The vibration signal method is a commonly used monitoring method for working conditions [11]. Mark et al. [12] investigated the early detection of gear based on vibration signals. Lin et al. [13] proposed a torsional-vibration analysis system for monitoring the internal combustion engine shaft system. Hassani et al. [14] systematically reviewed the development history of structural monitoring technology by observing its advantages and disadvantages. Sharma et al. [15] explored the monitoring and diagnosing of common faults in gearboxes from the frequency domain of vibration signals. In this way, the vibration response signal of the system can reflect the load excitation characteristics of the system by relying on transmission [16]. However, this single-source signal method may also have shortcomings. For example, a single type of signal can lead to poor robustness of feature signals due to differences in measurement point layout or monitoring methods. Furthermore, the harsh rolling production environment can easily lead to insufficient monitoring of source information and low recognition accuracy [17]. Simultaneously, during the research process in related fields, the author noticed the method of motor current signal analysis (MCSA) in the field of motors [18]. In other words, the stator current of the system will also change accordingly under variable load conditions [19]. Furthermore, MSCA is a state monitoring method based on motor current for monitoring, analyzing, and evaluating the stator current signal of the motor, making it easier to obtain the signal [20]. Gu et al. [21,22] conducted in-depth research in this field. Ahonen et al. [23] and Han et al. [24] also employed the MCSA method to measure the working data of centrifugal pumps. This study considers expanding the scope of signal objects and replacing single-source with multi-source signals (vibration signals and motor current signals) to increase the system's effective input information. Information fusion can obtain better and timely state evaluations as a multi-level method for interconnecting, processing, and combining multi-source data resources [25,26]. For example, Saimurugan et al. [27] fused acceleration signals with sound signals to solve mechanical fault problems. He et al. [28] introduced the history and development of the information fusion method by focusing on several representative key technologies. Feres et al. [29] explored multi-sensor collaborative detection in the air and conducted Neyman Pearson experiments. Safizadeh et al. [30] used the information fusion method for fault diagnosis of rolling bearings and achieved better evaluation results than a single sensor. Therefore, information fusion can integrate multi-source information, improve the coverage and effectiveness of available information, and optimize the recognition effect of payloads [31,32].

Based on the above analysis and considerations, the disciplinary advantage methods, such as the motor current method and information fusion method, are combined with load recognition of the rotor system based on the vibration method, constructing a new interdisciplinary intersection. Namely, the vibration and motor current response signals are fused in this paper, and information fusion methods are employed to recognize the rotor system load qualitatively. In this way, each single source of information can complement each other in value by achieving coordinated optimization of multi-source information, improving the availability and confidence of comprehensive information [28]. Therefore, the proposed method can obtain more accurate load recognition results than a single piece of information, revealing a more comprehensive system load status. Lastly, the proposed method has theoretical and practical significance for equipment operation safety and product quality improvement [31].

The subsequent sections of this paper are structured as follows. Section 2 introduces the theoretical basis of the methods proposed in this paper, namely the principles of signal reinforcement preprocessing and information fusion methods. In Section 3, the load recognition for the rotor system is described in detail by taking the measured signals as the object. Furthermore, comparing single and multi-source signal methods demonstrates that the information fusion method has additional advantages in recognizing payloads. Finally, some conclusions are drawn, and the paper is summarized in Section 4.

2. Methods and principles

This section mainly introduces the theoretical basis of the proposed methods. It mainly includes two parts: Section 2.1 and Section 2.2. Section 2.1 elaborates on the enhanced preprocessing method for the response signals of the rotor system, i.e., the singular value decomposition (SVD) and energy feature extraction by the wavelet packet. In Section 2.2, the origin, characteristics, and types of information fusion method are first introduced. Then, the selection of specific fusion methods is elaborated, along with the Bayesian estimation method in the feature-level fusion adopted in this paper.

2.1. Signal preprocessing method

Mixed response signals are formed due to the interference factors in the operation of the connecting-shaft rotor system, weakening effective information. Therefore, performing signal reinforcement preprocessing before conducting fusion analysis on the response signal is necessary.

2.1.1. Singular value decomposition

The first method used here is the SVD method, which reconstructs the original signal, i.e., only retaining the parts above a certain singular value [33]. In other words, this method can achieve information denoising and perform signal preprocessing [34].

If the rank of the matrix $A \in R^{m\times n}$ is $r > 0$, then there are orthogonal matrices V and U (corresponding to n-th and m-th orders, respectively). There is $A = U\begin{bmatrix} \sum & 0 \\ 0 & 0 \end{bmatrix} V^H$. Moreover, $\sum = diag(\sigma_1, \sigma_2, \cdots, \sigma_r)$, $\sigma_i (i = 1, 2, \cdots, r)$ is a singular value and $\sigma_1 \geq \sigma_2 \geq \cdots \geq \sigma_r > 0$. The singular values with higher magnitudes are located in the front, largely covering the information in A. Establishing the attractor matrix is crucial in the SVD process, which can be achieved by conversing the original signals.

$$A = [y_1 \quad y_2 \quad \cdots \quad y_m]^T = \begin{bmatrix} x_1 & x_2 & \cdots & x_n \\ x_2 & x_3 & \cdots & x_{n-1} \\ \cdots & \cdots & \cdots & \cdots \\ x_m & x_{m+1} & \cdots & x_{n+m-1} \end{bmatrix} \tag{1}$$

Matrix A can also be obtained using the following equation:

$$A = [z_1 \quad z_2 \quad \cdots \quad z_m] = \begin{bmatrix} x_1 & x_2 & \cdots & x_n \\ x_{n+1} & x_{n+2} & \cdots & x_{2n} \\ \cdots & \cdots & \cdots & \cdots \\ x_{(m-1)n+1} & x_{(m-1)n+2} & \cdots & x_{mn} \end{bmatrix} \tag{2}$$

2.1.2. Wavelet packet energy feature extraction

The wavelet analysis method refines the frequency of the low-frequency part and the time of the high-frequency part of the signal. However, the wavelet analysis method usually only has good resolution ability in the signal's low-frequency range. This method can hardly perform good decomposition on approaching signals. On the other hand, the wavelet packet analysis (WPA) method can analyze wavelets and decompose the high-frequency range of signals [35]. Gomez et al., Li et al., and Yang et al. used WPA for effective signal analysis [36–38].

The WPA decomposition process is shown in Fig. 1. The top layer is $(0,0)$, while the next three layers are decomposed layer by layer. Node (i,j) in each layer corresponds to a corresponding frequency band, where i represents the level of decomposition and j represents the order of nodes located in that layer. For example, (3,7) in Fig. 1 represents the seventh node of the third layer in the decomposition structure.

Next, it is necessary to deduce the energy values at each node, which can be obtained by the wavelet coefficients x_{jk} of each node. The energy value E_{3j} at node $(3,j)$ is expressed as Eq. (3), with k representing the sampling point.

$$E_{3j} = \sum_{k=1}^{n} x_{jk}^2 \tag{3}$$

The energy ratio of this node is

$$P_j = E_{3j} \Big/ \sum_{j=0}^{7} E_{3j} \tag{4}$$

Then, a feature vector P comprising each node can be obtained based on Eq. (4):

$$P = [P_0, P_1, P_2, P_3, P_4, P_5, P_6, P_7] \tag{5}$$

2.2. Information fusion method

"Information fusion" originated in the military and gradually evolved into a constantly evolving interdisciplinary and cross-domain information processing method [31]. This method fully integrates and utilizes information from multiple-sources (or sensors) by removing redundancy and complementary information to fuse and generate new valuable information. Hence, a more comprehensive description of the research object can be obtained [39,40].

Specifically, the characteristics of information fusion methods can be summarized as follows:

(1) Coverage: compared to single-source signal methods, multiple-source signals can fully integrate the information advantages of each source after being analyzed by fusion methods. Moreover, multiple source signals can restore and strengthen the signal's original characteristics to the maximum extent, improving the certainty and speed of target recognition. (2) Robustness: the fusion information method integrates multiple-sources of signals when a certain input signal is suddenly abnormal. Therefore, the final discrimination effect of the overall system is better and more reliable than the single-source information method. (3) Economy: using fusion methods means replacing difficult-to-obtain signals with some easily obtainable ones for analysis, reducing the overall experimental budget [41].

Information fusion methods can be divided into three types according to the different positions of the "fusion" stage in the entire

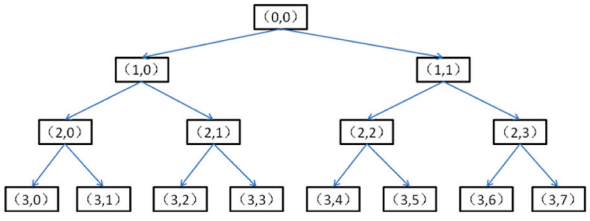

Fig. 1. Schematic diagram of wavelet packet decomposition. It decomposes layer by layer from the top to the bottom. The display here is a three-layer decomposition structure.

information fusion process: signal-level fusion, feature-level fusion, and decision-level fusion. The specific fusion method mentioned in this paper belongs to feature-level fusion.

Fig. 2 depicts a flowchart of the three methods mentioned above. The figure includes three subplots (a), (b), and (c), respectively showing three types of information fusion. The triangles in the figure represent the "fusion" stage, while the red, blue, and pink parts emphasize different positions where the "fusion" stage is located.

The red part in the left section (a) in Fig. 2 reflects signal-level fusion. The "fusion" stage starts fusion processing immediately after multiple signal input sources.

The blue part in the middle section (b) in Fig. 2 reflects feature-level fusion. First, feature extraction is performed separately for multi-source signals; then, coordinated "fusion" analysis is implemented through the fusion process.

The pink part in the right section (c) in Fig. 2 reflects decision-level fusion. The results are finally integrated through the "fusion" process once feature extraction and recognition analysis for multiple source signals are completed.

2.2.1. Selecting the specific method

Selecting specific fusion methods is a key consideration. The hierarchical structure of information fusion determines the corresponding applicable fusion methods [42]. The commonly used methods at different fusion levels are shown in Fig. 3. The three elliptical shapes in the middle of the figure represent three fusion types: signal-level, feature-level, and decision-level. Furthermore, fusion types are distinguished and sequentially marked in red, blue, and pink. Each type is further divided into its commonly used specific methods represented by boxes in the figure; their colors are consistent with their corresponding fusion type.

It is necessary to choose a method that is suitable for small sample online learning and for uncertain scenarios, based on the background of this research. Traditional statistical classification methods such as "maximum likelihood estimation" and "least squares" strongly depend on samples, i.e., they require a sufficiently large sample size. In other words, the advantages of these methods can only be demonstrated in large sample sizes. However, during actual operation, relatively little sample information can usually be obtained due to the limitations of experimental conditions. Machine learning methods have a wide range of applications, but they also have some limitations. Table 1 lists the relevant explanations. It is found by comparison that Bayesian estimation in feature-level fusion algorithms based on statistical thinking is an excellent small-sample statistical method. Moreover, the D-S evidence theory (another method of statistical thinking) is prone to the "Zadeh paradox" when encountering conflicting data. Therefore, Bayesian estimation is selected in this paper as the specific method for information fusion in recognizing the load type of the rotor system.

Many scholars have conducted in-depth research on Bayesian estimation in fusion methods and achieved beneficial results. In Ref. [43], an online Bayesian approach for fusing multi-resolution space-borne multispectral images was proposed. Experimental results indicate that the proposed strategy can lead to considerable improvements compared to both classical and state-of-the-art image fusion algorithms. Reference [44] proposed spatiotemporal information fusion approach based on Bayesian decision theory for land cover classification. The overall accuracy of Bayesian fusion for two cases rose by an average of 27.8 % compared with two single-source classifications. In Ref. [45], an experiment with 36-classes is carried out to evaluate and compare the performance of the fused, tactile, and kinesthetic perception systems. The results show that the Bayesian-based classifiers improves capabilities for object recognition and outperforms the Neural-based approach. Reference [46] predicts rock mass rating (RMR) ahead of the tunnel face with Bayesian estimation. This methodology is applied to the Laoying rock tunneling project in Yunnan Province, China. The findings demonstrate that the fusion of soft data and geological interpretation significantly improves the accuracy of the rock mass rating

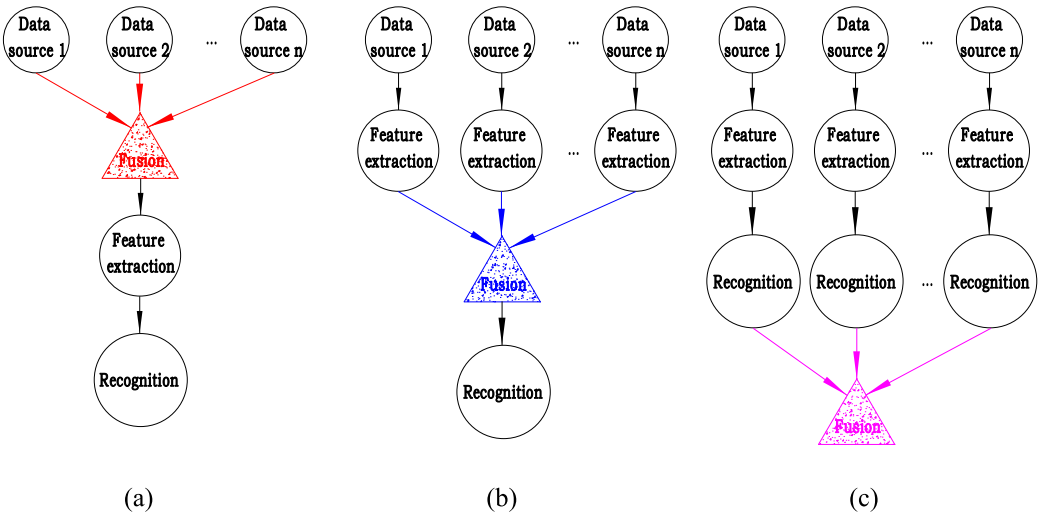

Fig. 2. Types of information fusion: (a) signal-level fusion, (b) feature-level fusion, (c) decision-level fusion. Each plot comprises four steps from top to bottom. The top layer is the "multi-source data layer", and the bottom layer requires a "feature extraction" step to perform "object recognition". The "information fusion" step is located at different positions among these three steps depending on the different fusion methods.

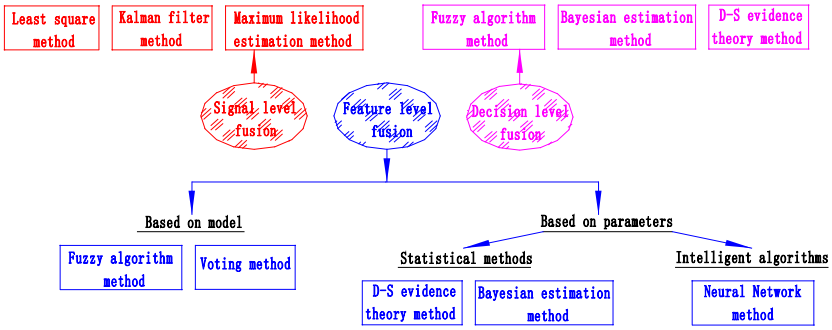

Fig. 3. Common information fusion methods. Some common and specific methods for each are listed according to the three types of information fusion in Fig. 2. For example, the Bayesian estimation method is a statistical method based on parameters in feature-level fusion.

Table 1
Comparison between Bayesian estimation and machine learning.

Comparison point	Bayesian estimation	Machine learning
Data volume requirements	Bayesian method can utilize prior distributions to compensate for insufficient data and improve the model's generalization ability, even in cases of small data volumes.	Many complex machine learning models, require a large amount of training data to avoid overfitting. When the amount of data is insufficient, these models find it difficult to generalize.
Risk of overfitting and online learning	Bayesian method is suitable for online learning or incremental learning. When new data arrives, the model can be gradually updated without retraining. This is particularly useful in dynamic environments that require real-time updates.	Complex models are prone to overfitting, meaning they perform well on training data but poorly on new data. Regularization and other techniques are usually required to avoid overfitting, which increases the difficulty of model design.
Uncertainty handling	Bayesian estimation naturally deals with uncertainty. It not only provides prediction results, but also the confidence level of the results, which is very important for decision-making.	Most machine learning models do not directly provide uncertainty estimates about the predicted results. However, in many cases, such as fault diagnosis, understanding the uncertainty of predictions is also important.

predictions. At selected prediction points, the relative error of this method is less than 15 % when compared to the traditional Kriging method.

2.2.2. *Bayesian statistical thinking*

Bayesian theorem is the core foundation of Bayesian statistical thinking and the theoretical basis of Bayesian estimation methods [47,48]. The Bayesian theorem can be expressed as follows:

$$P(Y|X) = \frac{P(X|Y)\ P(Y)}{P(X)} \tag{6}$$

Eq. (6) represents the probability that random event Y may occur when random event X occurs. Eq. (6) also reflects the two components of Bayesian statistical thinking: a prior distribution and a posterior distribution. The former refers to a probability distribution of the population distribution parameter θ, which can be represented by P(X|Y). Typically, posterior distribution can be obtained via human construction and probability calculation. The training samples can be partially selected from the samples, and statistical inference θ can be performed afterward. The latter is obtained via Eq. (6) and represented by P(Y|X). Therefore, the sample distribution does not have to be considered, only P(Y|X). Bayesian statistics can directly infer in this manner [49,50].

2.2.3. *Classification method based on Bayesian estimation*

Using Bayesian estimation for load type recognition involves using partially collected vibration signals and motor current signals to obtain a prior distribution (the main parameters involved in the calculation are shown in Table 2). The probabilities of different load types can be solved by P(X|Y) and X. The obtained corresponding class of the maximum probability value is the recognized load type.

When a appears, the conditional probability of b_i is $P(b_i \mid a)$, $i = 1, 2, \ldots, n$. The element a_i in X can be the time series matrix of two

Table 2
Main calculation parameters.

Parameter	Expression
Feature attribute (mutually exclusive)	λ
Feature element	$a = \{\lambda_1, \lambda_2, \ldots, \lambda_q\}$
Response signal samples to be recognized	$X = \{a_1, a_2, \ldots, a_m\}$
Recognized load type	$Y = \{b_1, b_2, \ldots, b_n\}$

types of signals, while the element b_i in Y is the load type. The probability of various load types on the signal can be calculated using the data in X and the obtained prior distribution. The type with the highest probability can be determined as this signal's type.

The test and training samples maintain a mutually exclusive relationship in this paper. The conditional probability matrix for different feature attributes (independent of each other) under various categories is shown in Eq. (7):

$$\begin{bmatrix} P(\lambda_1|b_1) & P(\lambda_2|b_1) & \dots & P(\lambda_q|b_1) \\ P(\lambda_1|b_2) & P(\lambda_2|b_2) & \dots & P(\lambda_q|b_2) \\ & \dots & & \\ P(\lambda_1|b_n) & P(\lambda_2|b_n) & \dots & P(\lambda_q|b_n) \end{bmatrix} \tag{7}$$

According to the Bayesian theorem:

$$P(b_i|a) = \frac{P(a|b_i)\ P(b_i)}{P(a)} \tag{8}$$

If the denominator in Eq. (8) is taken as a constant value, the equation size only depends on the numerical value of its numerator.

$$P(b_i)P(a|b_i) = P(b_i)\prod_{j=1}^{m} P(\lambda_j|b_i) \tag{9}$$

The expression $P(b_k \mid a) = \max\{P(b_1 \mid a), P(b_2 \mid a), \ldots, P(b_n \mid a)\}$ can be obtained by substituting the value obtained from Eq. (9) into $P(b_i \mid a)$ in Eq. (8). Therefore, the classification evaluation of a can be determined by b_k.

2.2.4. Handling of special situations

In the above process, there may be a special case of zero frequency, namely $P(\lambda_i \mid b_j) = 0$, indicating that the conditional probability of the feature attribute λ_i under class b_j is 0. The process of Bayesian classification relies on all feature attributes by default, which greatly weakens the classification effect. Therefore, when this special situation occurs, smoothing processing should be carried out. The Laplace calibration concept is introduced here. A brief introduction to it is as follows.

In statistics, when calculating the probability of an event occurring based on training data, its frequency is 0 if the event has never appeared in the training data. This results in the probability of the event being estimated as 0. This situation can lead to the model being unable to correctly evaluate new data points, as it may ignore features that have not appeared in the training set. Therefore, the core idea of Laplace calibration is to add a small positive value to each possible event, ensuring that no probability is absolutely zero. Simultaneously, in order to maintain a total probability of 1, it is necessary to adjust the denominator accordingly to avoid the problem of zero probability caused by zero frequency. When using frequency-based Bayesian classification, this calibration can assist in handling attribute values that have not appeared in the feature vectors.

Specifically, assuming there are r different categories, the number of times each category G_s appears in the training data is N_s, and the total number of training samples is N. Usually, the frequency of this category is used to estimate the probability $P(G_s) = N_s/N$; the calibrated probability estimate is $P(G_s)=(N_s+1)/(N + r)$. In this way, even if N_s is 0, the probability estimate will not be 0, but equal to $1/(N + r)$ which is a very small but non-zero probability value. However, this process requires recalculating the probabilities of all parts, which increases the workload. Therefore, the Laplace calibration has been improved here by assigning a very small probability to feature attributes that have 0 occurrences in the category. For example, a conditional probability matrix before calibration is [1 0 0], which becomes [0.98 0.01 0.01] after calibration. In this way, after calibration, zero frequency can be prevented from occurring, ensuring that every possible event has a non-zero probability estimate; and it helps to improve the generalization ability of the model, especially when the new data contains events that have not appeared in the training data.

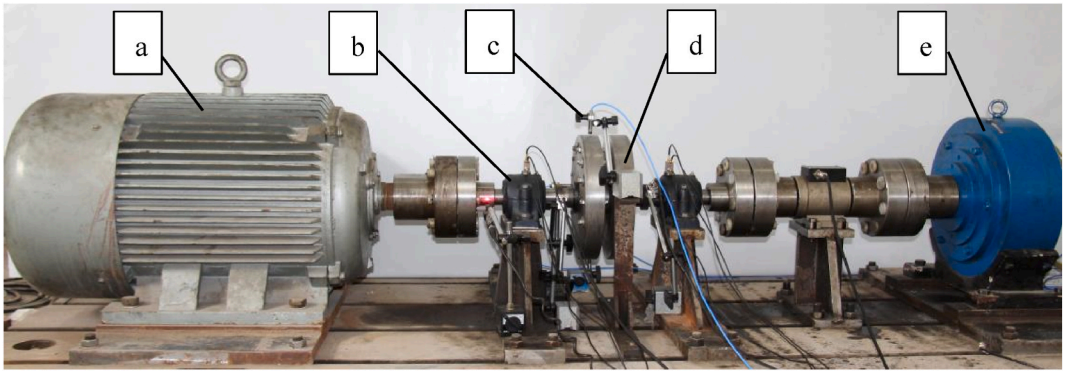

Fig. 4. Load recognition test-bed. Main components of the test-bed: (a) motor (connecting current transformer used to measure motor current); (b) bearing; (c) eddy current displacement sensor; (d) rotor; (e) magnetic powder brake.

3. Load recognition

This section mainly focuses on load recognition, qualitatively aiming at the measured signals of the rotor system. Section 3.1 introduces the load recognition test-bed and the acquisition of measured signals. In Section 3.2, preprocessing work is carried out on the response signals of the load recognition test. Section 3.3 explains the process of load recognition from three aspects: selecting feature attributes of the measured signals, prior statistical distribution, and analysis of recognition results. The theoretical principle corresponding to "3.2 Signal preprocessing" is described in Section 2.1; the theoretical principle corresponding to "3.3 Qualitative recognition process" is described in Section 2.2.

3.1. Obtaining measured signals

The response signals used in this paper were obtained through load recognition experiments. The main equipment used in the experiments is shown in Fig. 4. The basic experimental process involves applying load to the rotor system through the controller and the magnetic powder brake. Systematic loading tests are conducted multiple times according to the different types and parameters of external loads designed for the experiments. The INV3060 signal acquisition instrument was selected to synchronously sample the vibration information (in the x, y, and z directions) and the motor's current information of the rotor system, with a sampling frequency of 2048 Hz. The impact load needs to be maintained for 0.2 s. In this way, it is possible to reverse-recognize various load types originally loaded through the measured load response information.

A total of six rounds (twenty-four times) rotor system loading tests were conducted here (including four loading types: steady, linear, impact, and harmonic), based on the common loading conditions on the connecting-shaft rotor system. Experimental loads are shown in Table 3. In the equation in Table 3, M represents the torque excitation of the test, and t represents time. From each type of load form, three different parameters are selected randomly to obtain a total of twelve test data sets (motor current signals and vibration signals). These data sets are used as training samples. The data from the remaining twelve tests are used as test samples.

3.2. Signal preprocessing

In order to better understand the frequency components and features of the signal, frequency domain information is analyzed here. For example, a 85 Nm harmonic load and a 85 Nm impact load are applied separately to the rotor system to obtain the corresponding response signals, namely the motor current signals and vibration signals. Subsequently, the following preprocessing is performed on these signals.

As shown in Fig. 5, the displacement signal spectra in the x-direction are presented. There is not much difference in the frequency and amplitude of the vibration signal spectra of various loads. The main frequency component is the rotational frequency of 25 Hz, and there are smaller amplitude frequency components near the rotational frequency. Simultaneously, the frequency components near the frequency conversion under different load excitations have certain differences, but the amplitude of these frequencies is much smaller than that of 25Hz. These signal characteristics are difficult to analyze and observe, specifically, the load information is obscured by the strong frequency conversion signal.

The frequency spectra of motor current under load excitation are shown Fig. 6. The main frequency component in the two subplots is the 50Hz power frequency. There are smaller amplitude frequency components next to the power frequency component. There are certain differences in the frequency components exhibited under different load excitations. These signal characteristics are not obvious, specifically, the characteristic information is obscured by the strong power frequency signal, so it is not easy to recognize the loads at this time.

Frequency domain signals are preprocessed. SVD is performed to obtain the vibration signal spectrum (Fig. 7 shows the x-direction) and the current signal spectrum (Fig. 8). The signal morphology after SVD presents multiple characteristic frequencies, indicating that SVD can significantly weaken the main frequency effect and display other frequency components. However, a certain degree of main frequency effect can still be observed.

In order to observe the frequency distribution in more detail, a three-layer wavelet packet decomposition is performed on the signal frequency spectrum. For instance, the wavelet packet decomposition spectra of the current signal under 85Nm harmonic load are shown in Fig. 9. This figure illustrates the frequency spectrum of each node after each layer decomposition. Among them, the third layer decomposition presents the situation at eight nodes from node (3,0) to node (3,7). The load signals under other different parameters follow the same principle.

Subsequently, energy feature extraction is performed based on the signal spectra obtained at the eight nodes of the third layer. The

Table 3
Load excitation in the load recognition test.

Load type	Expression (Nm)					
Impact	$M = 25$	$M = 40$	$M = 55$	$M = 70$	$M = 85$	$M = 100$
Linear	$M = 0.5t+25$	$M = 0.5t+40$	$M = 0.5t+55$	$M = t+70$	$M = t+85$	$M = t+100$
Steady	$M = 25$	$M = 40$	$M = 55$	$M = 70$	$M = 85$	$M = 100$
Harmonic	$M = \sin4\pi t +25$	$M = 2\sin4\pi t +40$	$M = 2\sin4\pi t +55$	$M = 5\sin4\pi t+70$	$M = 5\sin4\pi t+85$	$M = 5\sin4\pi t+100$

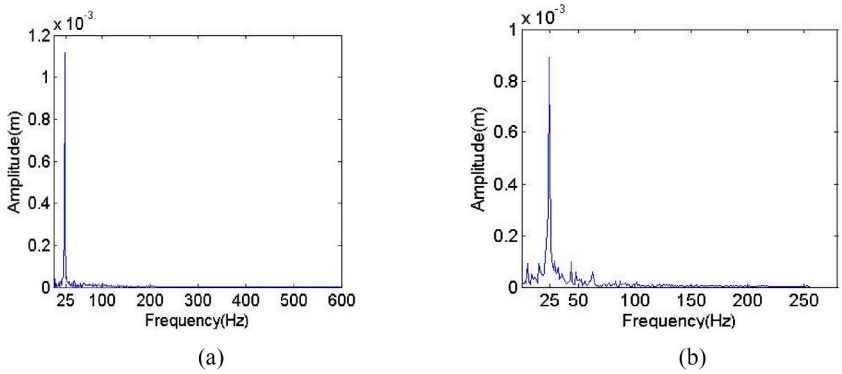

Fig. 5. Spectra of the *x*-direction vibration signals. (a) It is under a harmonic load of 85Nm. (b) It is under an impact load of 85Nm.

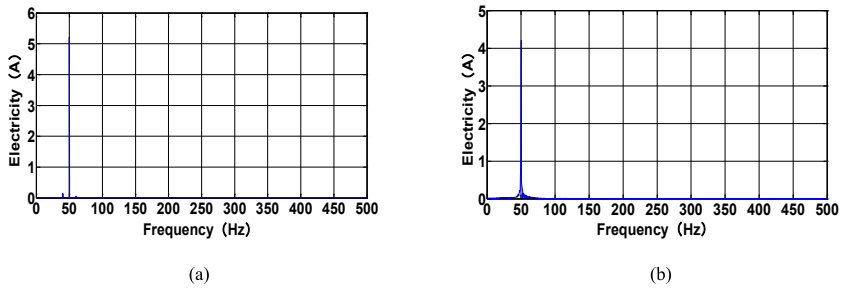

Fig. 6. Spectra of the stator current signals. (a) It is under a harmonic load of 85Nm. (b) It is under an impact load of 85Nm.

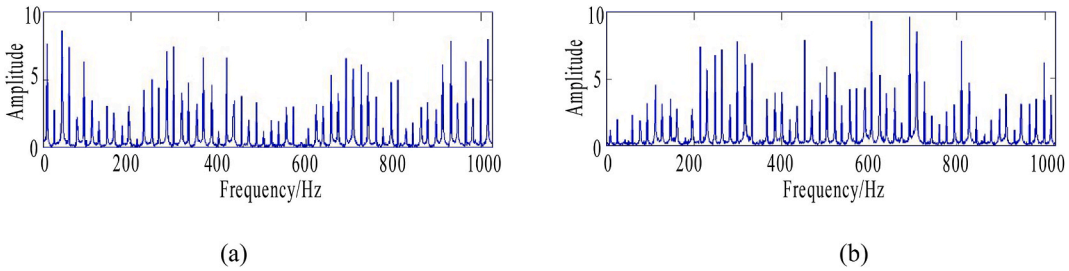

Fig. 7. Spectra of the *x*-direction vibration signals processed by SVD. (a) It is under a harmonic load of 85 Nm. (b) It is under an impact load of 85 Nm. The shape of the corresponding signal spectrum also varies under different types of loads.

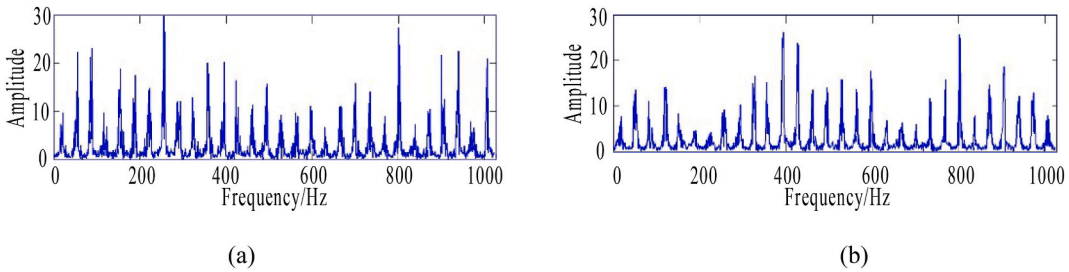

Fig. 8. Spectra of current signals processed by SVD. (a) It is under a harmonic load of 85 Nm. (b) It is under an impact load of 85 Nm. The shape of the corresponding signal spectrum also varies under different types of loads.

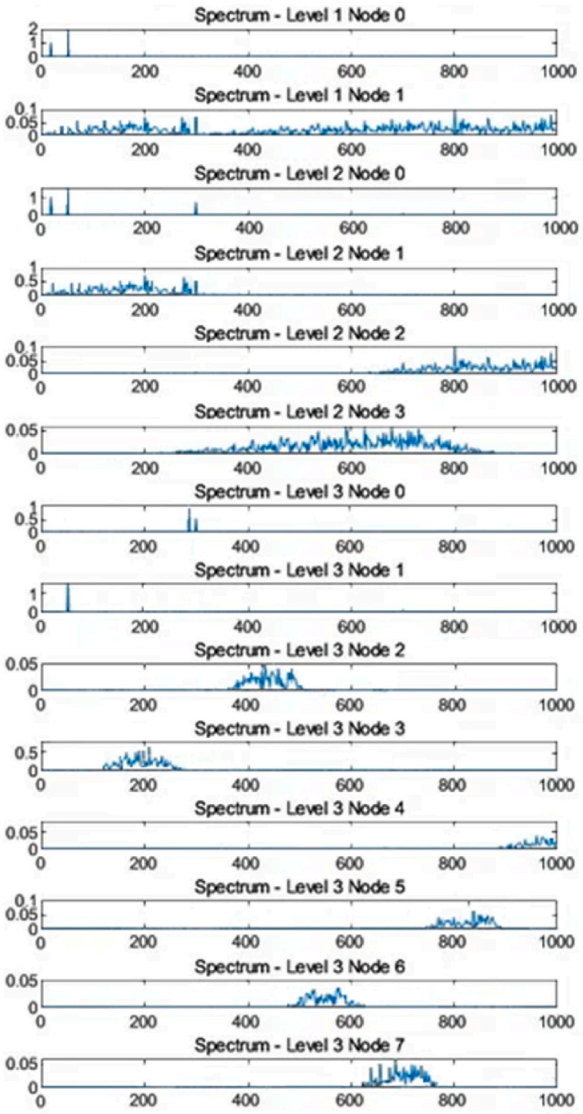

Fig. 9. Wavelet packet decomposition spectrum. The figure shows the current signal under a harmonic load of 85Nm.

energy distribution of the vibration signal (Fig. 10 shows the *x*-direction) and the energy distribution of the current signal (Fig. 11) are obtained using the wavelet packet method. The figures' energy distribution fluctuates and has different shapes, reflecting different effects of various loads on the response signal.

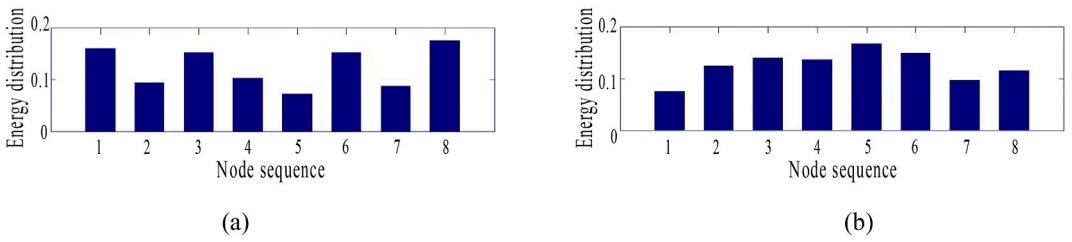

Fig. 10. Energy distribution of the *x*-direction vibration signals extracted by wavelet package. (a) It is under a harmonic load of 85 Nm. (b) It is under an impact load of 85 Nm. The energy distribution of the corresponding signal varies under different types of loads.

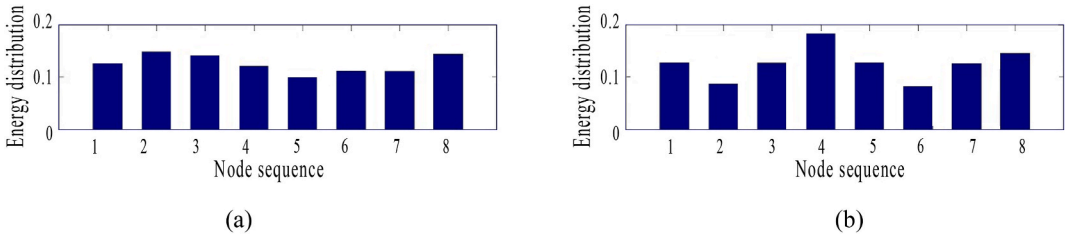

Fig. 11. Energy distribution of current signals extracted by wavelet package. (a) It is under a harmonic load of 85 Nm. (b) It is under an impact load of 85 Nm. The energy distribution of the corresponding signal varies under different types of loads.

3.3. Qualitative recognition process

This section focuses on the measured signals and specifically introduces the load recognition process of the rotor system with respect to the following three aspects.

3.3.1. Selecting feature attributes

Three different parameters from each type of load form are selected and used as training samples (motor's current and vibration signals from twelve times tests). After the preprocessing stage in Section 3.2, it is necessary to extract the feature values that can reflect the signal characteristics. According to the energy distribution diagram, the morphological changes exhibited differ. Moreover, differences in the distribution diagrams of different response signals (vibration signals, current signals) can also be observed. Subsequently, the two signal types can be complementary and organically integrated through information fusion methods, improving the signal performance.

In Bayesian estimation, the "attribute interval of feature objects" refers to the possible range of parameter values. The "feature object" is the object or variable being studied, while the "attribute interval" is the range of possible values for that object or variable. In the Bayesian statistical framework, this interval can correspond to the support domain of the prior distribution or the confidence interval of the posterior distribution. The current signal in this paper is taken as an example. After signal preprocessing, the energy distribution of current signals under different types of loads is the feature object; one feature attribute of the selected object is λ_1; the attribute intervals are three value ranges defined based on the distribution characteristics of the λ_1 values from all the training samples. In other words, these intervals can reflect the distribution characteristics of signal feature attributes under different loads.

Given observational data, the selection of feature attribute intervals in Bayesian estimation typically depends on specific requirements and data characteristics. In the Bayesian statistical framework, features can be divided into multiple intervals, which can be based on equal width (each interval covers the same numerical range) or equal frequency (each interval contains the same number of observations). When handling classification problems, intervals can be dynamically selected based on the importance of the features and the natural breakpoints among feature values, in order to better describe the data distribution.

Table 4 lists the feature attributes and their attribute intervals of the selected sample signals. Two characteristic attributes are selected for the motor current signal: λ_1 represents the ratio of the maximum node energy value to the minimum node energy value; λ_2 represents the sum of the energy values of node 2 and node 3. According to the characteristics of the sample signal, its attribute interval is divided into $\lambda_1 = \{\lambda \leq 1.7;\ 1.7 < \lambda < 2.0;\ \lambda \geq 2.0\}$; $\lambda_2 = \{\lambda \leq 0.22;\ 0.22 < \lambda < 0.25;\ \lambda \geq 0.25\}$. Based on the characteristics of the vibration signal, two feature attributes can be selected: λ_3 represents the ratio of energy between node 5 and node 6; λ_4 represents the ratio of the maximum node energy value to the minimum node energy value. Its attributes are divided into $\lambda_3 = \{\lambda \leq 1.05;\ 1.05 < \lambda < 1.34;\ \lambda \geq 1.34\}$; $\lambda_4 = \{\lambda \leq 1.74;\ 1.74 < \lambda < 2.40;\ \lambda \geq 2.40\}$.

3.3.2. Prior statistical distribution

Under four loading condition types, the analysis and solution are based on the node energy distribution of current information. The conditional probability matrix can be obtained for each feature attribute partition under each category, as shown in Eq. (10). This matrix is obtained based on twelve training samples (current) with three samples taken for each of the four types of loads. Bayesian estimation here is a matrix comprising two sets of conditional probabilities. The first to third columns of the matrix represent the conditional probability of feature attribute λ_1, corresponding to the three intervals of λ_1 in sequence. In contrast, the fourth to sixth columns represent the conditional probability of feature attribute λ_2, corresponding to the three intervals of λ_2 in sequence. Each row of

Table 4
Feature attributes of samples.

Signal type	(1) Motor current		(2) Vibration	
Feature	λ_1	λ_2	λ_3	λ_4
Meaning	The ratio of the maximum node energy value to the minimum node energy value	The sum of energy value of Node 2 and Node 3	The ratio of energy value between node 5 and node 6	The ratio of the maximum node energy value to the minimum node energy value
Attribute interval	$\{\lambda \leq 1.70;\ 1.70 < \lambda < 2.00;\ \lambda \geq 2.00\}$	$\{\lambda \leq 0.22;\ 0.22 < \lambda < 0.25;\ \lambda \geq 0.25\}$	$\{\lambda \leq 1.05;\ 1.05 < \lambda < 1.34;\ \lambda \geq 1.34\}$	$\{\lambda \leq 1.74;\ 1.74 < \lambda < 2.40;\ \lambda \geq 2.40\}$

the matrix corresponds to a type of load, from top to bottom being harmonic, impact, steady and linear. In each row, the first three numbers represent the probabilities of the training sample's feature attribute values occurring within the three intervals of λ_1, and the sum of these three numbers is 1; the last three numbers represent the probabilities of the training sample's feature attribute values occurring within the three intervals of λ_2, and the sum of these three numbers is 1.

Using the example of the 85Nm impact load in Fig. 10 (b). Its λ_1 value is 2.192, falling in the right segment of the attribute interval $\{\lambda \geq 2.0\}$ in Table 3, and its conditional probability corresponds to 0.333 in the second row and third column of Eq. (10). Its λ_2 value is 0.216, falling in the left segment of the attribute interval $\{\lambda \leq 0.22\}$ in Table 3, and its conditional probability corresponds to the second row and fourth column of Eq. (10). Due to the fact that the λ_2 values of the other two samples under impact load also fall within the left interval, the value at the second row and fourth column is "1".

$$\begin{bmatrix} 1 & 0 & 0 & 0 & 0 & 1 \\ 0 & 0.667 & 0.333 & 1 & 0 & 0 \\ 0.333 & 0.667 & 0 & 0.333 & 0 & 0.667 \\ 0 & 0.667 & 0.333 & 0 & 1 & 0 \end{bmatrix} \tag{10}$$

In Eq. (10), there is a special case where $P(\lambda_i \mid b_j) = 0$ is a zero frequency, representing that the conditional probability of feature attribute λ_i is 0 for a class b_j. Bayesian classification relies on all feature attributes by default, greatly weakening the classification effect. Therefore, Laplace calibration is required to obtain:

$$\begin{bmatrix} 0.980 & 0.010 & 0.010 & 0.010 & 0.010 & 0.980 \\ 0.020 & 0.657 & 0.323 & 0.980 & 0.010 & 0.010 \\ 0.323 & 0.657 & 0.020 & 0.323 & 0.020 & 0.657 \\ 0.020 & 0.657 & 0.323 & 0.010 & 0.980 & 0.010 \end{bmatrix} \tag{11}$$

Next, vibration information is analyzed and solved. The conditional probability matrix can be obtained for each feature attribute partition under each category, as shown in Eq. (12). Here, Bayesian estimation her is also a matrix comprising two sets of conditional probabilities. The first to third columns of the matrix represent the conditional probability of feature attribute λ_3. In contrast, the fourth to sixth columns represent the conditional probability of feature attribute λ_4.

$$\begin{bmatrix} 0.083 & 0.584 & 0.333 & 0.417 & 0.250 & 0.333 \\ 0.333 & 0.417 & 0.250 & 0.417 & 0.417 & 0.166 \\ 0.667 & 0.083 & 0.250 & 0.250 & 0.667 & 0.083 \\ 0.750 & 0.083 & 0.167 & 0.167 & 0.750 & 0.083 \end{bmatrix} \tag{12}$$

3.3.3. Results and discussion

3.3.3.1. Recognition results of the fusion method. The other half of the experimental data is randomly selected as the test sample and made mutually exclusive with the training sample to ensure good generalization performance. For example, the load recognition method is illustrated based on information fusion via the qualitative recognition process of an 85 Nm harmonic load. Under this load, the corresponding response signals (vibration signals in three directions and current signals) are taken as known conditions and subjected to the preprocessing to obtain the node energy distribution:

$$\begin{aligned} &\{0.130, 0.108, 0.146, 0.110, 0.141, 0.109, 0.118, 0.122\}, \\ &\{0.139, 0.087, 0.149, 0.130, 0.126, 0.088, 0.102, 0.172\}, \\ &\{0.155, 0.091, 0.145, 0.099, 0.073, 0.145, 0.082, 0.168\}, \\ &\{0.123, 0.141, 0.136, 0.117, 0.095, 0.108, 0.107, 0.136\}. \end{aligned} \tag{13}$$

The following expression can be obtained: $\lambda_1 = 1.484, \lambda_2 = 0.277; \lambda_3 = 1.076, \lambda_4 = 1.877$.
Therefore,

$$\begin{aligned} &P(a|Y = \text{Harmonic}) = 0.980 \times 0.980 \times 0.584 \times 0.250 = 0.14021840, \\ &P(a|Y = \text{Impact}) = 0.020 \times 0.010 \times 0.333 \times 0.417 = 0.00002777, \\ &P(a|Y = \text{Steady}) = 0.323 \times 0.657 \times 0.083 \times 0.667 = 0.01174821, \\ &P(a|Y = \text{linear}) = 0.020 \times 0.010 \times 0.083 \times 0.750 = 0.00001245 \ . \end{aligned} \tag{14}$$

The four load types are trained, ensuring that each type of load has the same number of training iterations: $P(Y = \text{Harmonic}) = P(Y = \text{Impact}) = P(Y = \text{Steady}) = P(Y = \text{Linear})$. According to Eq. (8):

$$\begin{aligned} P(Y = \text{Harmonic}|a) = \max\{&P(Y = \text{Steady}|a), P(Y = \text{Impact}|a), P(Y = \text{Harmonic}|a), \\ &P(Y = \text{Linear}|a)\} \end{aligned} \tag{15}$$

Therefore, according to these two types of response information, the qualitatively recognized result is consistent with the actual loading type in the experiment, i.e., the load type is in a "Harmonic".

3.3.3.2. Comparison of results between single and multi-source signal methods. For comparison purposes, the corresponding load recognitions are also carried out based on single-source vibration signals and single-source motor's current signals, respectively. The

qualitative recognition of 85 Nm harmonic load is taken as an example. The obtained results show that using the single-source vibration signals results in $P(a|Y = \text{Impact})$ maximum, indicating that the recognition result is an "impact load" and the result is incorrect. The single-source motor's current signals obtain the maximum value of $P(a|Y = \text{Harmonic})$, indicating that the recognition result is the "harmonic load" and the result is correct. Similarly, these three methods are used to recognize loads on 12 test samples qualitatively.

The recognition results of the four types of loads are shown in Table 5. The recognition accuracy of the motor's current method is 83.8 %, the recognition accuracy of the vibration method is 75.0 %, and the recognition accuracy of the fusion method is 91.7 %. These results indicate that the load recognition accuracy based on single source signals (motor current or vibration) is relatively low. A possible reason is that the selected number of operation samples is relatively small. Consequently, other test samples might be misevaluated, affecting the recognition accuracy. Furthermore, the selected feature attributes did not perfectly reflect the signal characteristics. The information fusion method improves these issues compared to single-source signal methods, resulting in higher recognition reliability.

The above comparative analysis shows that multi-source fusion methods can significantly improve the accuracy of load recognition. Furthermore, as the number of samples involved in the operation increases, the effectiveness of load recognition will be improved, and the final recognition accuracy of the fusion method will be better. Simultaneously, strengthening data mining and optimizing feature attributes to present signal characteristics perfectly can improve final recognition accuracy.

Due to space limitations, this study was unable to provide a comprehensive and multi angle analysis and introduction of "load recognition". It mainly includes the following two points. (1) Expansion of research direction in load recognition: this article mainly focuses on the type recognition of excitation loads and the characteristic analysis of their response information, and has not yet introduced other research directions in load recognition. (2) Expansion of application scenarios in load recognition: this article mainly focuses on the recognition research of several typical excitation loads, and can proceed to explore and discuss more complex special operating environments.

4. Conclusions

A fusion information method based on Bayesian estimation for the qualitative recognition of complex load types was proposed in this paper, addressing the limitations of single-type signals. The following conclusions are drawn:

Firstly, a signal reinforcement preprocessing method was obtained. In this paper, the components that reflect the load characteristics can be highlighted using singular value decomposition to eliminate the power frequency components in the vibration signal and current signal spectra. Digitalization of different load characteristics was achieved by utilizing the wavelet packet decomposition method to extract the spectral energy of the signal.

Secondly, effective payload recognition was achieved via the feature-level fusion method. In other words, the engineering problem of load recognition can be transformed into a mathematical problem by strengthening the preprocessed signals and using the Bayesian estimation method, achieving qualitative recognition of complex loads in a rotor system.

Finally, comparative results of single and multi-source signal methods were also obtained. Comparison of load recognition results between single and multi-source signal methods revealed that the fusion information method based on Bayesian estimation can overcome the shortcomings of a single signal, comprehensively coordinate multiple source signals, and improve the availability and confidence of information in time and space. Consequently, the detection and recognition ability of excitation loads are enhanced.

CRediT authorship contribution statement

Kun Zhang: Conceptualization, Data curation, Formal analysis, Funding acquisition, Methodology, Writing – original draft, Writing – review & editing. **Zhaojian Yang:** Conceptualization, Funding acquisition, Investigation, Methodology, Resources, Validation, Writing – review & editing.

Data availability

Data will be made available on request.

Declaration of competing interest

The authors declare the following financial interests/personal relationships which may be considered as potential competing interests:Zhaojian Yang reports financial support was provided by National Natural Science Foundation of China. Kun Zhang reports financial support was provided by Shanxi Provincial Department of Science and Technology. If there are other authors, they declare

Table 5
Comparison of different methods.

Method	Correct recognition number	Accuracy
Motor current	10	83.3 %
Vibration	9	75.0 %
Fuse information	11	91.7 %

that they have no known competing financial interests or personal relationships that could have appeared to influence the work reported in this paper.

Acknowledgment

This work was supported by National Natural Science Foundation of China (No. 51475318) and Basic Research Program of Shanxi Province (Natural Exploration) (No. 202103021223101). The authors also would like to thank MogoEdit (https://www.mogoedit.com) for its English editing during the preparation of this manuscript.

References

[1] Z.Y. Chen, Y. Liu, A. Valera-Medina, F. Robinson, Strip snap analytics in cold rolling process using machine learning, 2019 Ieee 15th, Int Conf Autom Sci Eng 9 (2019) 368–373, https://doi.org/10.1109/coase.2019.8842967.
[2] Y.R. Liu, L. Wang, Multiobjective-clustering-based optimal heterogeneous sensor placement method for thermo-mechanical load identification, Int. J. Mech. Sci. 253 (2023) 1–23, https://doi.org/10.1016/j.ijmecsci.2023.108369.
[3] C.Y. Fu, D.S. Shan, Q. Li, Damage location identification of railway bridge based on vibration response caused by vehicles, J. Southwest Jiao Tong Univ. 46 (2011) 719–725+769, https://doi.org/10.3969/j.issn.0258-2724.2011.05.002.
[4] J.Y. Zheng, J.Y. Tang, Z.X. Zhou, J.L. Heng, X. Chu, T. Wu, Intelligent cognition of traffic loads on road bridges: from measurement to simulation - a review, Measurement 200 (2022) 1–23, https://doi.org/10.1016/j.measurement.2022.111636.
[5] F. Xu, H.H. Chen, M. Bao, Force identification for mechanical vibration: state-of-the art and prospect, China Mech. Eng. 13 (2002) 526–531, https://doi.org/10.3321/j.issn:1004-132X.2002.06.024.
[6] Y.R. Liu, L. Wang, Quantification, localization, and reconstruction of impact force on interval composite structures, Int. J. Mech. Sci. 239 (2022) 1–23, https://doi.org/10.1016/j.ijmecsci.2022.107873.
[7] B. Movahedian, B. Boroomand, Inverse identification of time-harmonic loads acting on thin plates using approximated Green's functions, Inverse Probl Sci En 24 (2016) 1475–1493, https://doi.org/10.1080/17415977.2015.1124430.
[8] J.S. Hwang, D.K. Kwon, A. Kareem, Frequency domain identification of modal characteristics and loads from output-only measurements, Comput-aided Civ Inf 38 (2023) 2092–2108, https://doi.org/10.1111/mice.13011.
[9] F.D. Bartlett, W.G. Flannelly, Model verification of force determination for measuring vibratory loads, J Am Hellcopter Soc. 24 (1979) 10–18, https://doi.org/10.4050/JAHS.24.2.10.
[10] O.W. Petersen, O. Oiseth, E. Lourens, Investigation of dynamic wind loads on a long-span suspension bridge identified from measured acceleration data, J. Wind Eng. Ind. Aerod. 196 (2020) 1–16, https://doi.org/10.1016/j.jweia.2019.104045.
[11] Z.L. Wang, D.W. Shi, Y.D. Xu, D. Zhen, F.S. Gu, A.D. Ball, Early rolling bearing fault diagnosis in induction motors based on on-rotor sensing vibrations, Measurement 222 (2023) 1–15, https://doi.org/10.1016/j.measurement.2023.113614.
[12] W.D. Mark, H. Lee, R.J.D. Patrick, A simple frequency-domain algorithm for early detection of damaged gear teeth, Mech Syst Signal Pr 24 (2010) 2807–2823, https://doi.org/10.1016/j.ymssp.2010.04.004.
[13] Q. Lin, S.L. Yu, A portable digital torsional vibration analysis system and its signal processing, Adv. Mater. Res. 490–495 (2012) 1903–1907, https://doi.org/10.4028/www.scientific.net/AMR.490-495.1903.
[14] S. Hassani, U. Dackermann, A systematic review of advanced sensor technologies for non-destructive testing and structural health monitoring, Sensors 23 (2023) 1–83, https://doi.org/10.3390/s23042204.
[15] V. Sharma, A. Parey, Frequency domain averaging based experimental evaluation of gear fault without tachometer for fluctuating speed conditions, Mech Syst Signal Pr 85 (2017) 278–295, https://doi.org/10.1016/j.ymssp.2016.08.015.
[16] J.H. Cao, Z.B. Yang, R.B. Sun, G.R. Teng, OPR-free single probe blade tip timing for monitoring rotating blade, Int. J. Mech. Sci. 247 (2023) 1–22, 10.1016/10.1016/j.ijmecsci.2023.108174.
[17] P. Nazarko, L. Ziemiański, Application of elastic waves and neural networks for the prediction of forces in bolts of flange connections subjected to static tension tests, Materials 13 (2020) 3607, https://doi.org/10.3390/ma13163607.
[18] M.S. Rafaq, M.F. Shaikh, Y. Park, S.B. Lee, Reliable airgap search coil based detection of induction motor rotor faults under false negative motor current signature analysis indications, Ieee T Ind Inform 18 (2022) 3276–3285, https://doi.org/10.1109/TII.2020.3042195.
[19] M.H. Farhat, L. Gelman, A.O. Abdullahi, A. Ball, G. Conaghan, W. Kluis, Novel fault diagnosis of a conveyor belt mis-tracking via motor current signature analysis, Sensors 23 (2023) 1–18, https://doi.org/10.3390/s23073652.
[20] G. Niu, X. Dong, Y.J. Chen, Motor fault diagnostics based on current signatures: a review, Ieee T Instrum Meas 72 (2023) 1–19, https://doi.org/10.1109/TIM.2023.3285999.
[21] F. Gu, Y. Shao, N. Hu, A. Naid, A.D. Ball, Electrical motor current signal analysis using a modified bispectrum for fault diagnosis of downstream mechanical equipment, Mech Syst Signal Pr 25 (2011) 360–372, https://doi.org/10.1016/j.ymssp.2010.07.004.
[22] F. Gu, Y. Shao, N. Hu, A. Naid, A.D. Ball, Electrical motor current signal analysis using a modified bispectrum for fault diagnosis of downstream mechanical equipment, Mech Syst Signal Pr 25 (2011) 360–372, https://doi.org/10.1016/j.ymssp.2010.07.004.
[23] T. Ahonen, J.T. Kortelainen, J.K. Tamminen, J. Ahola, Centrifugal pump operation monitoring with motor phase current measurement, Int J Elec Power. 42 (2012) 188–195, https://doi.org/10.1016/j.ijepes.2012.04.013.
[24] Y.J. Han, J.P. Yuan, Y. Luo, J.M. Zou, Operation Diagnosis for Centrifugal Pumps Using Stator Current-Based Indicators, vol. 237, P I MECH ENG C-J MEC, 2022, pp. 1075–1087, https://doi.org/10.1177/09544062221126637.
[25] Z.H. Hong, P.F. Sun, R.Y. Zhou, X.H. Tong, Y.J. Feng, S.J. Liu, Fast mosaicking method of InSAR-generated multi-stripe digital elevation model, J Infrared Millim W 41 (2022) 493–500, https://doi.org/10.11972/j.issn.1001-9014.2022.02.016.
[26] A. Sharma, G.K. Patra, V.P.S. Naidu, Bispectral analysis and information fusion technique for bearing fault classification, Meas. Sci. Technol. 35 (2024) 1–13. http://10.1088/1361-6501/acffe4.
[27] M. Saimurugan, R. Ramprasad, A dual sensor signal fusion approach for detection of faults in rotating machines, J. Vib. Control 24 (2018) 2621–2630, https://doi.org/10.1177/1077546316689644.
[28] Y. He, X. Guan, G.W. Wang, Survey on the proogress and prospect of multisemor information fusion journal of astronautics, J Astronaut. 26 (2005) 524–530, https://doi.org/10.3321/j.issn:1000-1328.2005.04.028.
[29] C. Feres, B.C. Levy, Z. Ding, Over-the-air multisensor collaboration for resource efficient joint detection, Ieee T Signal Proces 72 (2024) 384–399, https://doi.org/10.1109/TSP.2023.3310895.
[30] M.S. Safizadeh, S.K. Latifi, Using multi-sensor data fusion for vibration fault diagnosis of rolling element bearings by accelerometer and load cell, Inform Fusion. 18 (2014) 1–8, https://doi.org/10.3321/10.1016/j.inffus.2013.10.002.
[31] Z.Q. Han, J.J. Yu, N.X. Li, Z.Y. Wabg, Overview of information fusion technology, J. Intell. 29 (2010) 110–114, https://doi.org/10.3969/j.issn.1002-1965.2010.z1.036.
[32] W.L. Wang, Y. Gao, Pipeline leak detection method based on acoustic-pressure information fusion, Measurement 212 (2023), https://doi.org/10.1016/j.measurement.2023.112691.

[33] M. Chiyonobu, T. Miyamae, M. Takata, J. Harayama, K. Kimura, Y. Nakamura, Singular value decomposition for complex matrices using two-sided Jacobi method, J. Supercomput. 2 (2024) 1–22, https://doi.org/10.1007/s11227-024-05903-6.
[34] R. Golafshan, K.Y. Sanliturk, SVD and Hankel matrix based de-noising approach for ball bearing fault detection and its assessment using artificial faults, Mech Syst Signal Pr 70–71 (2016) 36–50, https://doi.org/10.1016/j.ymssp.2015.08.012.
[35] X.L. Liu, J. Han, H.W. Xu, X.B.A. Xiao, Z.F. Wen, S.L. Liang, An indirect method for rail corrugation measurement based on numerical models and wavelet packet decomposition, Measurement 191 (2022) 1–14, https://doi.org/10.1016/j.measurement.2022.110726.
[36] M.J. Gomez, C. Castejon, E. Corral, M. Cocconcelli, Railway axle early fatigue crack detection through condition monitoring techniques, Sensors 23 (2023) 1–20, https://doi.org/10.3390/s23136143.
[37] Z.Z. Li, P.X. Gao, D.Z. Zhao, J.R. Liu, Application of wavelet packet and fractal combination technology in analyzing aero-engine hydraulic pipeline vibration signals with variable pressure, Comput Eng Sci 38 (2016) 807–813, https://doi.org/10.3969/j.issn.1007-130X.2016.04.028.
[38] J.T. Yang, M.Y. Zhao, Z.Q. Zhang, P.K. Li, Traction motor bearing fault detection via wavelet packet analysis of stator currents, J China Railway Soc. 35 (2013) 32–36, https://doi.org/10.3969/j.issn.1001-8360.2013.02.006.
[39] G. Niu, T. Han, B.S. Yang, A.C.C. Tan, Multi-agent decision fusion for motor fault diagnosis, Mech Syst Signal Pr 21 (2007) 1285–1299, https://doi.org/10.3321/10.1016/j.ymssp.2006.03.003.
[40] C. Feres, B.C. Levy, Z. Ding, Over-the-air multisensor collaboration for resource efficient joint detection, Ieee T Signal Proces 72 (2023) 384–399, https://doi.org/10.1109/TSP.2023.3310895.
[41] M. Saimurugan, R. Ramprasad, A dual sensor signal fusion approach for detection of faults in rotating machines, J. Vib. Control 24 (2018) 2621–2630, 107754631668964.
[42] L.B. Ascari, A.S. Costa, A bad data resilient multisensor fusion framework for hybrid state estimation, Ieee T Power Syst. 39 (2024) 132–146, https://doi.org/10.1109/TPWRS.2023.3261201.
[43] H.Q. Li, B. Duvvuri, R. Borsoi, T. Imbiriba, E. Beighley, D. Erdogmus, P. Closas, Online fusion of multi-resolution multispectral images with weakly supervised temporal dynamics, Isprs J Photogramm 196 (2023) 471–489. https://10.1016/j.isprsjprs.2023.01.012.
[44] Y. Jin, X.D. Guan, Y. Ge, Y. Jia, W.M. Li, Improved spatiotemporal information fusion approach based on Bayesian decision theory for land cover classification, Rem. Sens. 14 (2022) 6003. https://10.3390/rs14236003.
[45] F. Pastor, J. García-González, J.M. Gandarias, D. Medina, P. Closas, A.J. Garcia-Cerezo, J.M. Gómez-de-Gabriel, Bayesian and neural inference on LSTM-based object recognition from tactile and kinesthetic information, IEEE Robot Autom Let. 6 (2021) 231–238. https://10.1109/LRA.2020.3038377.
[46] X.J. Li, Z.Y. Chen, L. Tang, C. Chen, T. Li, J.X. Ling, Y.Y. Lu, Y. Rui, Predicting rock mass rating ahead of the tunnel face with Bayesian estimation, Front Earth Sc-Switz 12 (2024) 333117. https://10.3389/feart.2024.1333117.
[47] H. Takahashi, Bayesian definition of random sequences with respect to conditional probabilities, Inform Comput 292 (2023) 13, https://doi.org/10.1016/j.ic.2023.105041.
[48] S.S. Afshari, F. Enayatollahi, X.Y. Xu, X.H. Liang, Machine learning-based methods in structural reliability analysis: a review, Reliab Eng Syst Safe 219 (2022) 1–31, https://doi.org/10.1016/j.ress.2021.108223.
[49] H. Seo, Y.S. Kang, M. Bennis, W. Choi, Bayesian inverse contextual reasoning for heterogeneous semantics-native communication, Measurement 72 (2024) 830–844, https://doi.org/10.1109/TCOMM.2023.3327771.
[50] M. Jean, P. Granier, T. Leroy, Experimental evaluation of a Bayesian estimation and control of engine knocking level, Ieee T Contr Syst T 31 (2023) 1934–1940, https://doi.org/10.1109/TCST.2023.3247194.